Solid Earth, 7, 917–927, 2016
www.solid-earth.net/7/917/2016/
doi:10.5194/se-7-917-2016

Solid Earth Open Access EGU

X-ray CT analyses, models and numerical simulations: a comparison with petrophysical analyses in an experimental CO_2 study

Steven Henkel[1], Dieter Pudlo[1], Frieder Enzmann[2], Viktor Reitenbach[3], Daniel Albrecht[3], Leonhard Ganzer[3], and Reinhard Gaupp[1]

[1]Institute of Geosciences, Friedrich Schiller University Jena, 07749 Jena, Germany
[2]Institute for Geosciences, Johannes Gutenberg University Mainz, 55122 Mainz, Germany
[3]Institute of Petroleum Engineering, Clausthal University of Technology, 38678 Clausthal-Zellerfeld, Germany

Correspondence to: Steven Henkel (henkel.steven@uni-jena.de)

Received: 25 February 2016 – Published in Solid Earth Discuss.: 8 March 2016
Revised: 11 May 2016 – Accepted: 21 May 2016 – Published: 7 June 2016

Abstract. An essential part of the collaborative research project H2STORE (hydrogen to store), which is funded by the German government, was a comparison of various analytical methods for characterizing reservoir sandstones from different stratigraphic units. In this context Permian, Triassic and Tertiary reservoir sandstones were analysed. Rock core materials, provided by RWE Gasspeicher GmbH (Dortmund, Germany), GDF Suez E&P Deutschland GmbH (Lingen, Germany), E.ON Gas Storage GmbH (Essen, Germany) and RAG Rohöl-Aufsuchungs Aktiengesellschaft (Vienna, Austria), were processed by different laboratory techniques; thin sections were prepared, rock fragments were crushed and cubes of 1 cm edge length and plugs 3 to 5 cm in length with a diameter of about 2.5 cm were sawn from macroscopic homogeneous cores. With this prepared sample material, polarized light microscopy and scanning electron microscopy, coupled with image analyses, specific surface area measurements (after Brunauer, Emmet and Teller, 1938; BET), He-porosity and N_2-permeability measurements and high-resolution microcomputer tomography (μ-CT), which were used for numerical simulations, were applied. All these methods were practised on most of the same sample material, before and on selected Permian sandstones also after static CO_2 experiments under reservoir conditions. A major concern in comparing the results of these methods is an appraisal of the reliability of the given porosity, permeability and mineral-specific reactive (inner) surface area data. The CO_2 experiments modified the petrophysical as well as the mineralogical/geochemical rock properties. These changes are detectable by all applied analytical methods. Nevertheless, a major outcome of the high-resolution μ-CT analyses and following numerical data simulations was that quite similar data sets and data interpretations were maintained by the different petrophysical standard methods. Moreover, the μ-CT analyses are not only time saving, but also non-destructive. This is an important point if only minor sample material is available and a detailed comparison before and after the experimental tests on micrometre pore scale of specific rock features is envisaged.

1 Introduction

The globally rising carbon dioxide emissions associated with increasing climate extremes are intensively discussed by government authorities, scientists, industrial representatives and the public. The target of the intended so-called German *Energiewende* is a shift in energy production based on fossil fuels and nuclear power to renewable energy sources (e.g. wind, solar).

As part of these debates and transformation processes the German Federal Ministry of Education and Research (BMBF) funded the hydrogen to store project (H2STORE). One main objective of the research was to characterize mineral, synthetic formation fluid, microbiological and petrophysical interactions in reservoir sandstones, induced by

hydrogen and carbon dioxide autoclave batch experiments (Pudlo et al., 2013, 2015; Henkel, 2016). Such reactions were investigated by autoclave experiments at reservoir temperatures and pressures, using non-corrosive autoclaves and fluids similar to reservoir-specific formation fluids. To satisfy the need to reduce greenhouse gas emissions as per the Kyoto Protocol (1997) and most recently the UN climate conference in Paris in 2015, intentions to capture, inject and store CO_2 (CCS) in the geological underground are even more relevant. In particular, the geochemical and fluid chemical reactions of stored CO_2 and the geological underground, which occur under different reservoir conditions (p, T, x fluid), are not fully understood and need further research, primarily on the maximum pressure, temperature and formation water salinity conditions for potential CO_2 storage sites. Also, the utilization of CO_2 combined with H_2 injection into the geological underground for the "green methane" generation (Šmigiáň et al., 1990), enforced by microorganism activity (Panfilov, 2010), demands further research regarding the potential CO_2–biotic-mineral-formation-fluid reactions.

Additionally, the integrity of wells, including the behaviour of e.g. bore hole casings in a highly corrosive environment of H_2 / CO_2-gas mixtures is an essential consideration in the potential usage of the geological underground for storage options. This study contributes to these topics by analysing rock samples provided by the industrial partners RWE Gasspeicher GmbH (Dortmund, Germany), GDF Suez E&P Deutschland GmbH (Lingen, Germany), E.ON Gas Storage GmbH (Essen, Germany) and RAG Rohöl-Aufsuchungs-Aktiengesellschaft (Vienna, Austria). The samples are representative for different sandstone reservoirs and therefore different reservoir conditions.

High-resolution computed tomography (μ-CT) data associated with numerical fluid flow simulations using the GeoDict – Math2Market® modules and standard petrophysical analyses, which were conducted at the Technical University Clausthal before and after static autoclave experiments, were applied. Thus we verified potential reactions induced by the CO_2 autoclave experiments on the Permian sandstones and compared these data with the results, achieved by the other conventional petrophysical analytic methods (e.g. Pudlo et al., 2014).

2 Material

The used sandstones derive from areas and stratigraphic formations which comprise the main reservoir units in Germany and Austria. The sample material originates from three different stratigraphic units, (a) the Permian from the Altmark in north-eastern Germany, (b) the Triassic from the Emsland in north-western Germany and (c) the Tertiary from the Molasse of south Germany and north-western Austria (cf. Fig. 1 and Henkel et al., 2013). Therefore, the source areas, the detrital content, the depositional environment and the diagenetic evolution of these sediments are diverse, implying that the samples experienced different burial pressures, temperatures and interactions with their site-specific formation fluids. The current reservoir conditions of the sample sites of interest are summarized in Table 1, showing the marked differences, especially in regard to the Permian and Tertiary sample sites. The current burial depth of the Permian samples is about 3500 m with a reservoir temperature of 120 to 125 °C. This is in contrast to the recent Tertiary reservoir conditions with a burial depth of 1600 m and reservoir temperatures of about 40 °C (Table 1). Also, the formation fluid salinities range from 35.22 % salinity in the Permian reservoirs to only 1.81 % salinity in the Tertiary formation fluids. Table 2 presents the data on the handled sandstone samples along with the methods applied and the Permian material used for the CO_2 experiments.

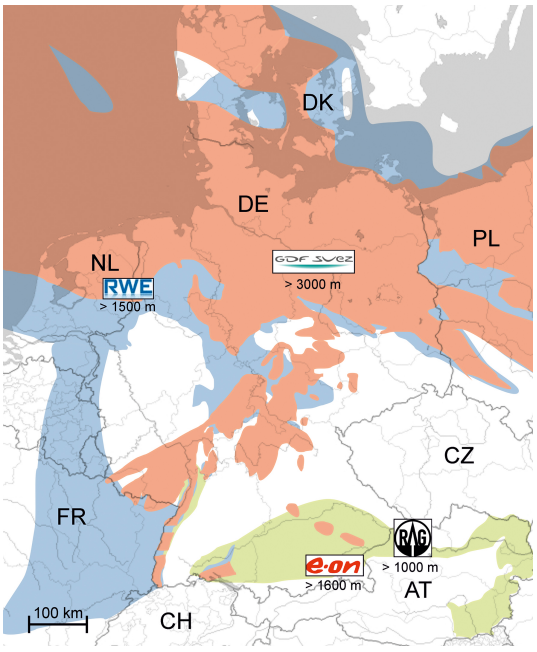

Figure 1. Location map of the study areas with information on reservoir depth and the company which provided sample material. The coloured outlined areas represent the distribution of strata in the underground of the potential reservoir units. In red the Permian, in blue the Triassic and in green the Tertiary strata are shown (adapted from Henkel et al., 2013).

Comparison of the detrital rock composition by petrographic thin-section analyses shows that a wide range of sandstone types is present because of the quartz, feldspar and lithoclast content of the different locations (Fig. 2, after McBride, 1963). The Permian samples are classified mainly as arkoses, subarkoses and quartz arenites; the Triassic sandstones vary from subarkoses, lithic subarkoses, sublitharenites to litharenites and the Tertiary samples comprise lithic subarkoses, sublitharenites, litharenites, lithic arkoses and feldspar litharenites.

Table 1. Overview of the recent reservoir conditions of the sampled locations.

Location	Stratigraphy	Recent burial depth	Recent temperature	Reservoir pressure	Salinity of formation fluid
Saxony-Anhalt	Permian	3500 m	125 °C	20 MPa	35.2 %
Lower Saxony	Triassic	1700 m	100 °C	10 MPa	28.8 %
Bavaria	Tertiary	1600 m	40 °C	10 MPa	1.8 %
Austria	Tertiary	1100 m	40 °C	10 MPa	3.5 %

Table 2. Sample overview and methods used for the presented data (A represents single analyses, B represents repeated method after CO_2 autoclave experiments with the same sample; X is outlining the samples used for these experiments).

Material		Thin sections	Plugs			Cube	Rock fragments
sample	stratigraphy	petrographic analyses	He-porosity	N_2-permeability	autoclave experiment	μ-CT	BET
C-1	Tertiary	A	A	A		A	
C-2		A	A	A			
C-3		A	A	A			
C-4		A	A	A			
C-5		A	A	A			
C-6		A	A	A			
C-7		A	A	A		A	
B-1	Triassic	A	A	A		A	A
B-2		A	A	A		A	A
B-3		A	A	A			
B-4		A	A	A			
B-5		A	A	A		A	
B-6		A	A	A		A	
B-7		A	A	A			
B-8		A	A	A		A	
A-1	Permian	A	A/B	A/B	X	A/B	A/B
A-2		A	A	A		A	
A-3		A	A/B	A/B	X	A/B	A/B
A-4		A	A	A			A
A-5		A	A	A	X		A/B
A-6		A	A	A			
A-7		A	A	A			
A-8		A	A	A	X	A/B	A/B
A-9		A	A	A	X		A/B
A-10		A	A	A	X	A/B	A/B

Moreover, the rocks contain varying amounts of pore-filling, framework-stabilizing cements like anhydrite, carbonate and exhibit different amounts of open pore space (Fig. 3), which all influence the fluid flow fields because of the different tortuosities of the pore network.

For the autoclave experiments and the petrophysical, mineralogical and chemical analyses, the core material from all locations was prepared as in Henkel et al. (2014). Thus the sandstone material for thin sections, plugs (3.0 to 5.0 cm in length, 2.5 cm in diameter), μ-CT cubes (1.0 cm edge length) and rock fragment (0.3 to 0.5 cm in diameter) preparation was sampled side by side in the homogeneous zones of the drill core material to guarantee the best possible comparability of the data generated by the different methods. This is the standard for reservoir material characterization. Examples of macroscopic homogeneous parts of the sampled drill cores are given in Fig. 4, in which different lithotypes of the reservoir material are also indicated. This will again influence the fluid flow or fluid migration characteristics of the reservoir sandstones and therefore the petrophysical properties, owing to the considerable tortuosities of the pore network. Thus a wide range of different rock compositions and qualities were

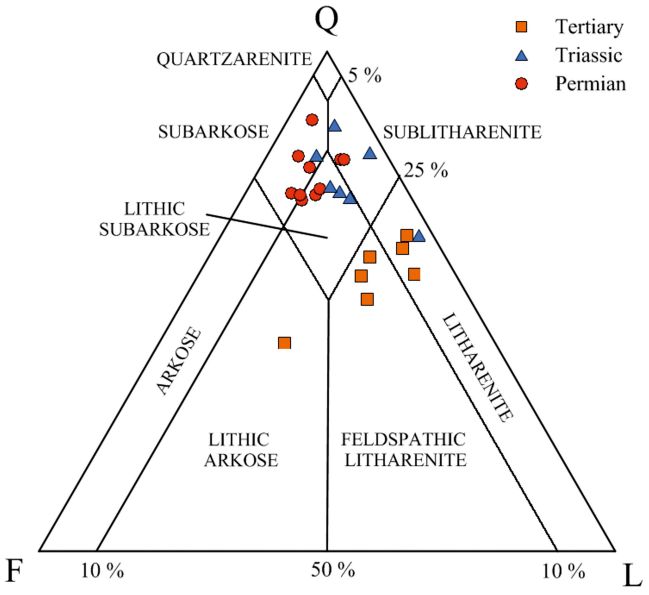

Figure 2. Petrographic sandstone classification after McBride (1963) for samples of this study. This petrographic classification was conducted by identifying and analysing 300 minerals in thin sections of the selected samples and plotting the determined quartz (Q), feldspar (F) and lithoclast (L) content in a ternary diagram. The different colours correspond to the different stratigraphic units and therefore locations (cf. Fig. 1, Table 2).

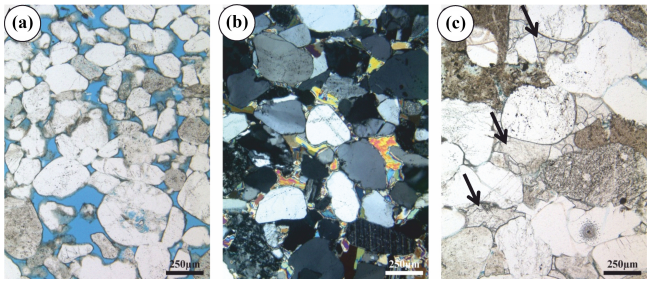

Figure 3. Thin-section images with 50× magnification given different diagenetic features (pore-filling cements) of the sandstone samples. In **(a)** a transmitted light image of a sample with free pore space is shown (blue represents open pore). In **(b)** an image of a thin section with crossed nicols is shown, highlighting pore-filling anhydrite cement (rainbow colours). In **(c)** a transmitted light image of a thin section with pore-filling carbonate cement is shown (arrows).

available for this study. Also, the grain sizes of the different sandstone samples varied from silt/fine sand to coarse sand (Fig. 5) fraction (Wentworth, 1922).

Thus the property differences of the various reservoirs influence their characteristics. In the CO_2 autoclave experiments under reservoir conditions, only the Permian samples were used, for capacity reasons. For all samples the following methods were applied and the outcomes of the different petrophysical methods were compared with the μ-CT-generated data.

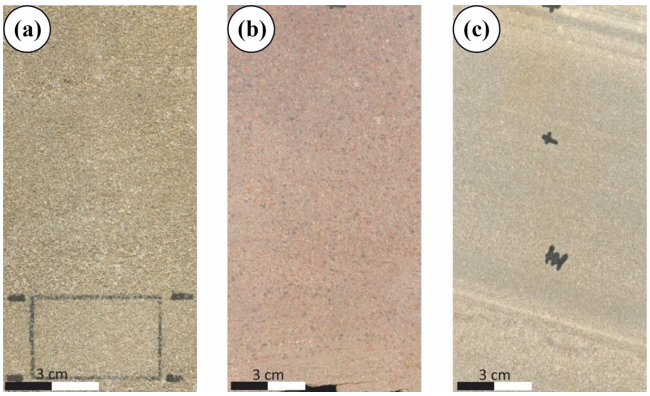

Figure 4. Different examples of lithotypes of the analysed Permian sandstones. In **(a)** a brownish, plane-horizontal stratified medium-grained sandstone type is shown. In **(b)** a red, massive, medium coarse-grained sandstone type is visualized and in **(c)** a greyish, obliquely bedded fine-medium-grained sandstone type is presented.

3 Methods

Analytical methods were applied to macroscopically homogeneous sandstones from the three stratigraphic formations on identical drill core material to compare the outcomes achieved by the different analytical methods. Additionally, the Permian samples were used for CO_2 experiments in sample-specific reservoir conditions and were analysed before and after these experiments at the same samples and marked sample positions respectively. Therefore, a pinpoint comparison of different mineral reactions owing to the CO_2 experiments was possible.

CO_2 autoclave batch experiments lasting between four and seven weeks were conducted at the Clausthal University of Technology (TU Clausthal) on rock-formation brine systems, at high pressure and high temperature (HPHT) with corrosion-resistant autoclaves and using selected thin sections, rock fragments, cubes and plugs (Pudlo et al., 2015; Henkel et al., 2015). Helium porosity and nitrogen permeability measurements before and after the tests were performed on sandstone plugs at TU Clausthal. For porosity analysis the set-up by Torsaeter and Abtahi (2003) was used and permeability determinations were conducted with a Hassler cell in an up- and downstream regime and calculated with Darcy's law equations.

The fluid samples of the formation fluids used in the two autoclave experiments (5 to 10 mL) were taken before, during and after the tests at TU Clausthal and were chemically analysed in terms of their major, minor and trace element contents at the Friedrich Schiller University Jena (FSU Jena).For the analyses with an error of about 1 %, an in-

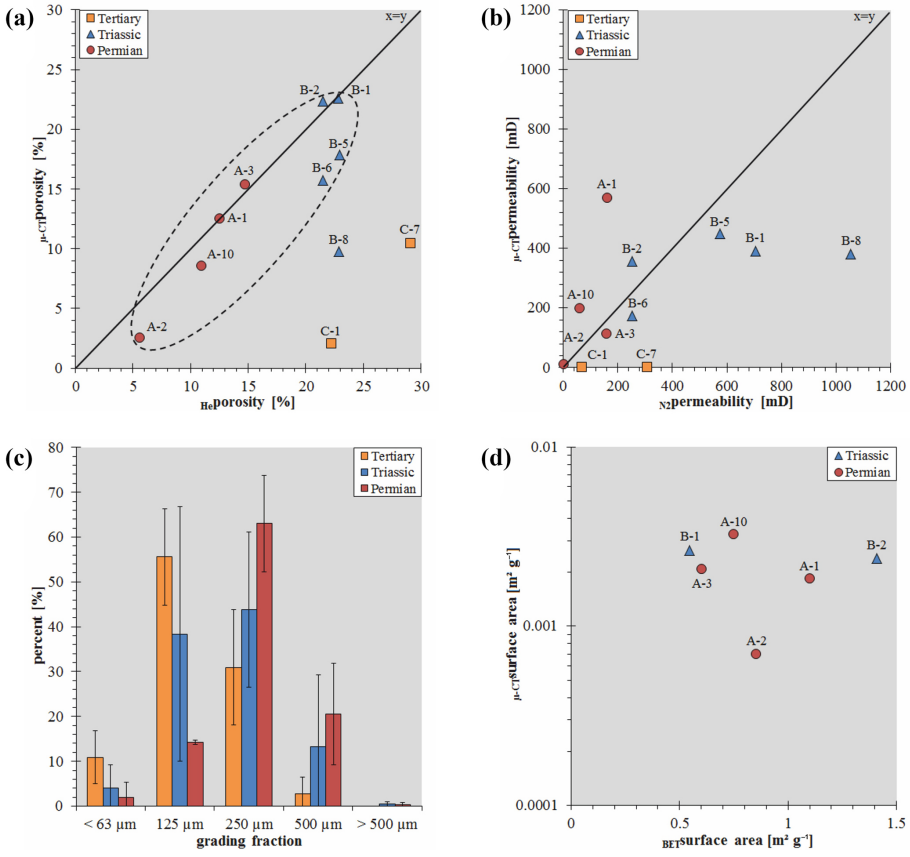

Figure 5. In **(a)** the porosity results of the same eleven μ-CT and He-porosity analysed samples are shown for the three different stratigraphic units. The ellipse marks the sandstone samples with coarse sand (2.00–0.63 mm) and medium sand (0.63–0.20 mm) grain sizes. In **(b)** the permeability data of the same sample set as shown in **(a)** are presented. In **(c)** the mean grain fraction sizes (after Wentworth, 1922) analysed on thin section with the corresponding standard deviation of the 25 samples in this study are shown (cf. Table 2). In **(d)** the mean values of the specific surface area data from the BET and μ-CT methods are outlined for Permian and Triassic samples.

ductively coupled plasma mass spectroscope combined with an optical emission spectroscope (ICP-MS/OES) of Thermo Fischer (Scientific X Series II) were used. Also, the physicochemical characterization of the formation fluid was conducted in the laboratories of the Institute of Geoscience in Jena. PHREEQC 3.3 software (Parkhurst and Appelo, 2013) and a database for highly saline fluids (Pitzer et al., 1984) were used to calculate the saturation indices of the fluids for the pore-filling minerals (carbonate and anhydrite). Polarized light microscopy and field-emission scanning electron microscopy (FE-SEM) were used at FSU Jena for the mineralogical investigations. Thereby a Zeiss Axioplan II petrological microscope, equipped with 10× magnification and objectives of 2.5×, 5×, 10×, 20×, 40× magnifications, was used. The microscope was combined with a mounted Hitachi HV-C20 digital camera for high-resolution thin-section documentation. An SMT ULTRA plus field-emission scanning electron microscope from Carl Zeiss Enterprises, coupled with an energy-dispersive X-ray (EDX) detector and the analytical software of Bruker AXS Microanalysis GmbH, was used for mineral documentation and identification.

A Procon CT Alpha 160 device at Johannes Gutenberg University Mainz was used for high-resolution computer tomography. The detector resolution was about 2048×2048 pixels. The parameters were 100 kV of voltage and a current of 80 µA. Scans were performed at 0.45° steps over a total rotation range of 360°. The achieved resolution for the different sample material was between 7.6 and 8.6 µm per voxel. Sandstone cubes with an edge length of 1.0 cm were scanned. The reconstruction of the scans was performed with the Octopus 7.0® software. The μ-CT image adaptation with anisotropic diffusion filtering and pore space segmentation was performed with Avizo® fire 7.1 software. Intense distinct beam hardening was corrected with the software MATLAB® and the approaches based on Jovanovic et al. (2013). For the calculations of porosity, surface area, fluid flow and deduced permeability, the corresponding modules PoroDict and FlowDict of the software package GeoDict (Math2Market®) were used (Wiegmann, 2007; Wiegmann et

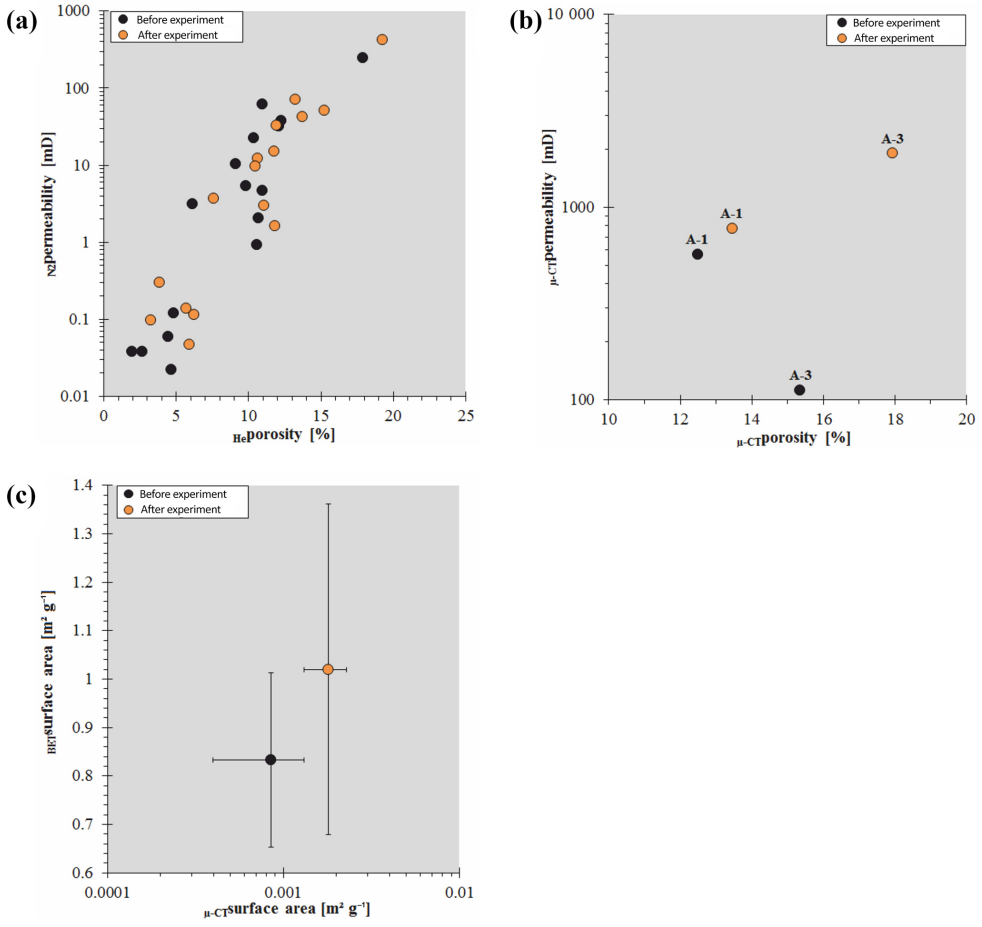

Figure 6. In **(a)** the helium porosity and nitrogen permeability measurement results of 16 Permian samples before and after CO_2 experiments are presented (data from Pudlo et al., 2012). In **(b)** the μ-CT porosity and μ-CT permeability data for two Permian cube samples before and after the CO_2 experiments are shown. In **(c)** the mean values of the measured BET surface areas (six samples) and the calculated μ-CT surface areas (four samples) before and after the CO_2 experiments are shown.

al., 2013). Therefore the calculated surface areas from the μ-CT data correlated with the volume and weight of the corresponding sandstone cube. The Navier–Stokes–Brinkman flow solver in FlowDict and density properties of water at 20 °C were used for the fluid flow simulation and permeability calculations.

The specific surface area (BET) measurements for gently crushed rock fragments were determined following Brunauer et al. (1938) at the Technical University of Munich before and after the experimental runs with exactly the same sample material. Therefore the representable sandstone material adjacent to the plugs, thin sections and cubes was used and broken by a press into fragments with a diameter of about 0.3 to 0.5 cm. This material was separated by a ripple divider to produce 5 to 7 g of sample material for the analyses. This material was shipped for BET analyses, and selected Permian samples after the measurements were used for the CO_2 experiments before the BET analyses were repeated to detect any surface area variation caused by the autoclave experiments. FE-SEM analyses of the crushed sample surfaces were partly conducted after sample preparation to identify any crack generation. No such artificial cracks were detected at the sample surfaces up to nanometre scale.

4 Results

The initial state of the statistical porosity, permeability and specific surface area data, determined by the different methods of this study, is shown in Fig. 5. The measured helium porosity and nitrogen permeability values for the Permian plug samples ranged from 5.64 to 14.73 % and from 2.61 to 161.32 mD respectively. For the measured Triassic samples, the helium porosity data ranged between 11.02 and 29.95 % and nitrogen permeability data between 251.93 and 1609.43 mD. The measured Tertiary plug samples represent porosity values of 19.14 to 26.62 % and permeability values from 25.80 to 388.00 mD. The corresponding parameters calculated from the μ-CT data with PoroDict and FlowDict in

the GeoDict software produced porosity values of 2.55 to 15.36 % and permeability values of 8.56 to 570.28 mD for the Permian samples. For the Triassic samples porosities of 9.79 to 22.57 % and permeability values ranging from 18.41 to 449.09 mD were computed. The Tertiary samples had calculated porosities of 0.52 to 10.41 %. Lack of flow connectivity (no connected pore networks in the Tertiary samples were detected) meant that modelling of permeability from CT data was not possible for these samples.

The specific surface area measured by the BET method after Brunauer et al. (1938) of crushed rock fragments of the Permian samples revealed values of 0.64 to 2.34 $m^2\,g^{-1}$ and for the Triassic samples values ranging from 0.45 to 1.72 $m^2\,g^{-1}$. The calculated surface area from the CT data sets ranged from 0.0018 to 0.0033 $m^2\,g^{-1}$ for the Permian sandstones and from 0.0006 to 0.0038 $m^2\,g^{-1}$ for the Triassic samples. The four Permian and two Triassic samples, which were cross-checked by the BET and μ-CT calculation methods, are outlined in Fig. 5d.

PHREEQC numerical simulations confirmed that because of the very high concentrations of Na^+, Ca^{2+} and Cl^- (Table 2) the used formation fluids are very close to saturation with respect to NaCl and $CaCO_3$ (Table 3). In contrast, this modelling suggests that anhydrite ($CaSO_4$) can be dissolved in these fluids, because of its slight undersaturation of sulfur (S). Because of the high ion concentrations in the synthetic brine, a very high electrical conductivity was measured (cf. Tables 2 and 3).

For the CO_2 experiments only sample material from Permian sandstones was used. The measured petrophysical data after the CO_2 experiments under sample-specific reservoir conditions from the selected 16 sandstone plugs ranged from 3.25 to 19.24 % for porosity and from > 0.01–419.60 mD for permeability (Fig. 6a). These data were compiled from identical sample material in a study by Pudlo et al. (2012). The calculated petrophysical data of two sandstone cube samples from μ-CT scans resulted in porosity of 10.43 and 17.93 % and permeability of 247.58 and 1909.05 mD (Fig. 6b).

To determine the specific surface area in six Permian samples (cf. Table 2), the BET method was used and values of 0.51 to 2.75 $m^2\,g^{-1}$ were revealed. In contrast, PoroDict-calculated real surface areas (after Ohser and Mücklich, 2000) from the μ-CT data sets of four Permian sample cubes with a volume of 1 cm^3 were lower. Here the estimated real surface areas ranged between 0.0017 and 0.0024 $m^2\,g^{-1}$ (Fig. 6c).

By comparing the calculated fluid flow fields before and after the CO_2 experiments (cf. Figs. 7a–b and 8a–b), we found an increase of fluid pathways related to enhanced porosity and permeability after the CO_2 tests. Regarding the FE-SEM and EDX results on thin sections (cf. Fig. 9), a dissolution of pore-filling anhydrite and carbonate cements was evident when we compared identical sample position before and after the CO_2 experiments (Fig. 9). The fluid chemical analyses after the CO_2 experiments indicated an increase of sulfur and a depletion of Na^+, Ca^{2+} and Cl^- (Table 3) in the formation fluid. Also, the pH and the electrical conductivity values decreased in the formation fluid after the CO_2 experiments (cf. Tables 3 and 4).

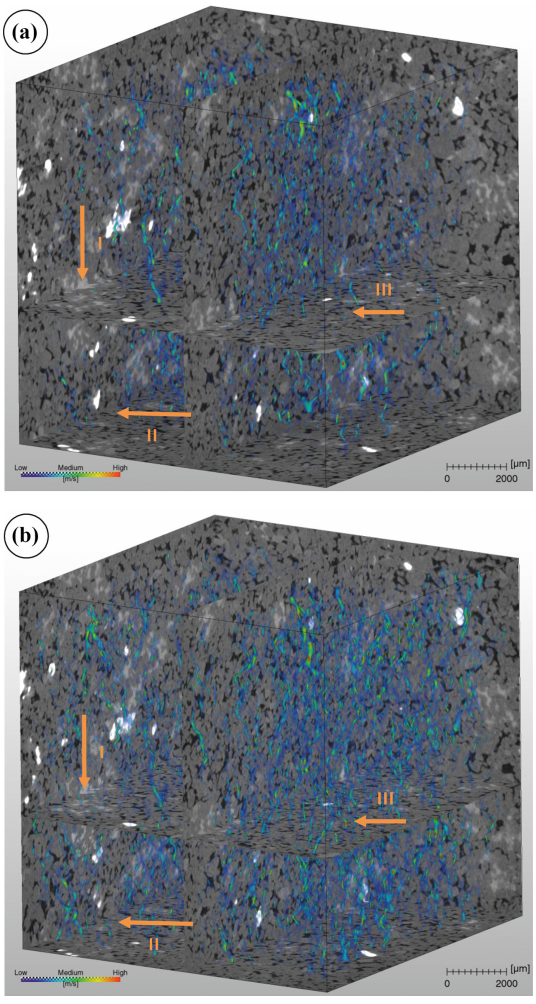

Figure 7. In **(a)** and **(b)** the details of the same Permian sandstone sample before **(a)** and after **(b)** the seven-week CO_2 experiments under reservoir conditions are shown. Note the reduction of the blocky cements (light grey) and therefore the fluid flow field with increased fluid migration pathways and rather higher migration velocities (blue to red colours) after the experiments **(b)**. This is verified by arrows I to III in a direct comparison of the same sample position before and after the CO_2 experiments.

The PHREEQC calculations (Table 4) regarding the data sets from the ICP-MS/OES analyses after the CO_2 experiments suggested supersaturation with respect to $CaCO_3$ in the formation fluids. The slight undersaturation of $CaSO_4$ (anhydrite) in the fluids was even further depressed during the CO_2 experiments.

Table 3. Results of formation fluid analyses (ICP-MS/OES) of selected ions and the corresponding physicochemical data of two Permian autoclave runs, before and after CO_2 experiments under static reservoir conditions. Because of the common stratigraphic origin the initial formation brine composition is similar for both samples.

	Before CO_2 experiments						After CO_2 experiments					
	Na^+ ($g\,L^{-1}$)	Ca^{2+} ($g\,L^{-1}$)	Cl^- ($g\,L^{-1}$)	S^{total} ($mg\,L^{-1}$)	pH	elec. cond. ($\mu S\,cm^{-1}$)	Na^+ ($g\,L^{-1}$)	Ca^{2+} ($g\,L^{-1}$)	Cl^- ($g\,L^{-1}$)	S^{total} ($mg\,L^{-1}$)	pH	elec. cond. ($\mu S\,cm^{-1}$)
S 1	65.53	54.27	203.80	7.50	9.45	45 700	7.05	6.15	22.24	247.00	6.71	6790
S 2							5.53	4.77	17.54	54.00	6.77	5370

Table 4. PHREEQC modelling, showing saturation results of the interaction of the synthetic formation fluid used before, during and after the CO_2 experiments exposed to the Permian sandstones (n.a. is not analysed, SI is the saturation index, pE is the negative logarithm of electron concentration directly proportional to the redox potential).

	P (MPa)	T (°C)	pH	pE	SI $CaCO_3$	SI $CaSO_4$	SI NaCl
Laboratory standard conditions before CO_2 experiments	0.1	20	9.54	6.7	0.48	−3.27	−1.35
Reservoir conditions during CO_2 experiments	25.0	120	3.23	6.7	−3.19	−4.09	−1.70
Laboratory standard conditions after CO_2 experiments	0.1	20	6.71	n.a.	−3.39	−4.93	−3.10

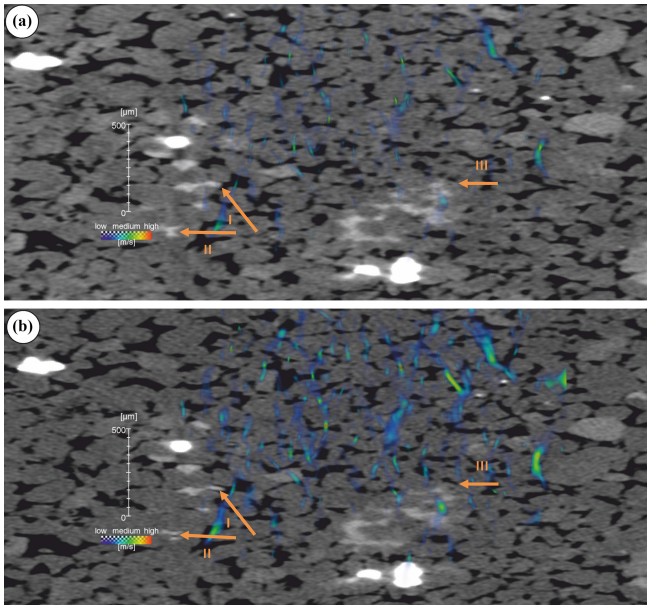

Figure 8. In **(a)** and **(b)** the identical Permian sandstone sample is presented before **(a)** and after **(b)** CO_2 experiments under reservoir conditions. The images are enhanced sections from Fig. 7 and verify the dissolution of the blocky pore-filling cements (arrows) and the enhanced fluid flow field and fluid flow velocities after the experiments resulting from the dissolution events (blue to red colours).

5 Discussion

The given comparison of the porosity data deduced by high-resolution computer tomography scans and measurements by helium porosity confirms that the two methods achieve very similar results (cf. Fig. 5). Nevertheless, the grain sizes of sandstones (cf. Fig. 5a, c) and the restricted resolution rate of the μ-CT scans of this sample influence the quality of the calculated porosity data. Results from the fine-grained and very fine-grained sandstone samples from the Tertiary and Triassic imply that the data of helium porosity measurements are more precisely due to helium intrusion even into micropores ($<7.6\,\mu m$ resolution of μ-CT) and thus the capability of helium to migrate even through very narrow pore throats. In contrast, because of the limited resolution of μ-CT scans (7.6 to 8.6 µm $voxel^{-1}$), such micropores are therefore not detectable and calculated porosities are marginally lower than those revealed by helium porosity measurements. These differences regarding micropores probably led to distinct porosity data in fine-grained to very fine-grained rocks, whereas porosity determinations on coarse- and medium-grained sandstone samples are similar in both methods. By comparing the results from identical samples after the CO_2 experiments, we found that both methods confirm the same increase in porosity. The mean helium porosity measurements revealed an increase in total porosity of 16.0 % and the calculated μ-CT data one of 12.6 % because of the CO_2 experiments. Thus, the effects on porosity characteristics after four to seven week-long CO_2 experiments under reservoir conditions are verified by both methods.

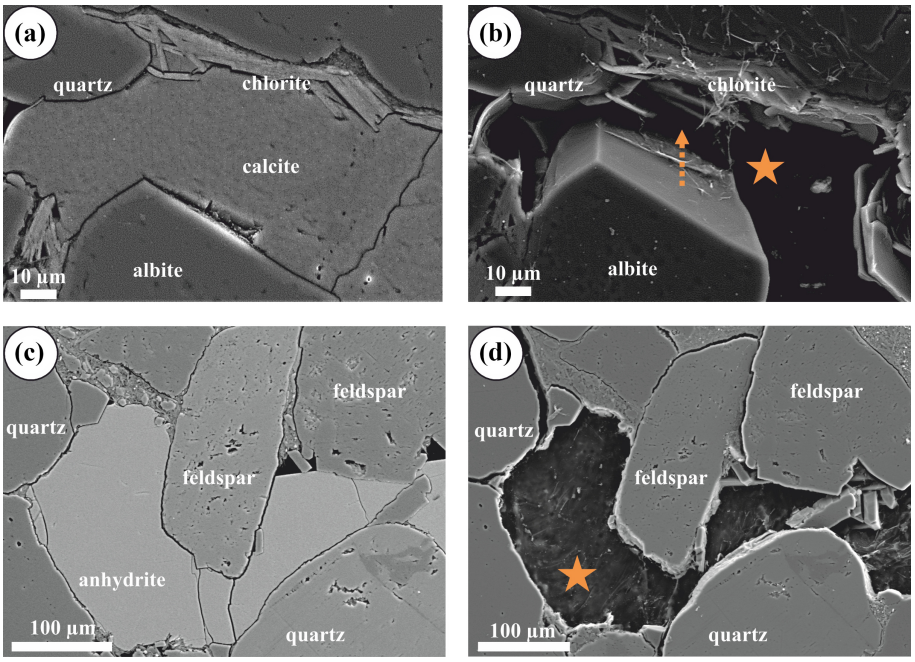

Figure 9. Secondary electron FE-SEM images of the same section of a Permian sandstone sample before **(a, c)** and after **(b, d)** CO_2 experiments under reservoir conditions for seven weeks. The dissolution of pore-filling calcite cement (star in **b**) and the exposure of grain rimming clay minerals (arrow in **b**) led to increasing porosity outcomes after the CO_2 experiments and the increase of the specific surface area (modified after Henkel et al., 2014). In **(c)** and **(d)** the dissolution of pore-filling anhydrite cement (star in **d**) is shown at exactly the same thin-section position before **(c)** and after **(d)** the CO_2 experiments, also leading to increasing porosity values after the experiments.

Also, the calculation of the surface areas using μ-CT data is limited by the restricted resolution of the μ-CT scans. However, the calculations by the GeoDict software can offer reference values. Nevertheless, the results of the specific surface area measurements after Brunauer et al. (1938) are more realistic if compared with sandstone data from the literature (see e.g. Pudlo et al., 2015) and for a direct comparison of the data from the same sample before and after the CO_2 experiments, the BET method is of great benefit (cf. Kieffer et al., 1999). Also, compared with the GeoDict approach, more reliable data were achieved with the BET method. The μ-CT calculations and GeoDict modules could profit by including additional parameters in the calculations such as rock/mineral densities, volume and the compositional as well as the morphological features of the pore space exposed mineral phases. Nevertheless an important outcome of comparing the data sets compiled before and after the CO_2 experiments is that both methods confirm an increase in surface area. The μ-CT investigations and calculations indicated an enhancement in the surface area of about 14.3 %, which is very similar to the 10.4 % maintained by the BET method. This is supported by the FE-SEM findings (Fig. 9) with an enhanced exposure of small grain rimming clay minerals (chlorite) to the pore space after the CO_2 experiments because of the dissolution of the former pore filling and the clay minerals blocking carbonate and anhydrite cements.

The measured nitrogen permeability data and the results from the μ-CT calculations by GeoDict are of the same order (cf. Fig. 5b). Nevertheless, the quality of calculated permeabilities from the μ-CT data sets is restricted to the resolution of the CT scan and therefore of the segmented pore space (pixel resolution: 7.6 to 8.6 µm). Here again the grain size of the scanned samples is a limiting factor combined with the scan resolution. While for coarse- and medium-grained sandstones, the results are most similar to the nitrogen permeability measurements, these resemblances are minimized with decreasing grain size. Nevertheless, by comparing the permeability data after the CO_2 experiments with the results before the experiments, we found that both methods confirmed a marked increase in permeability induced by the tests (cf. Fig. 6a, b). This increase is about 1.75 times higher in the calculations than in the nitrogen permeability measurements.

The fluid chemical analyses confirmed the petrophysical outcomes e.g. an increase of S^{total} in the formation fluids after the experiments which originated from the dissolution of the pore-filling anhydrite cements in the samples. This led to increased petrophysical properties (porosity, permeability, surface area) in the reservoir sandstone samples. The fluid flow simulations also indicated that, even when sampled in homogeneous drill core zones, the lithotypes and poikiloblastic texture of the cements (cf. Fig. 8) influenced the fluid migration pathways and their dissolution as the CO_2 experiments enhanced the reservoir quality.

Nevertheless, the heterogeneity of a sandstone sample within a few millimetres or centimetres can reveal different petrophysical characteristics or influence different geochemical or fluid chemical analyses compared with a sample alongside to the previous. This is of concern, especially in the analysis of different lithotypes in one reservoir unit, sandstone samples with poikiloblastic textures of pore-filling cements or sandstones with clay lenses.

6 Conclusions

This study confirms that high-resolution computer tomography is a suitable method for verifying data from petrophysical standard methods as well as for identifying alteration of various mineral phases of sandstone samples induced during CO_2 batch experiments. The benefit of analysing the same sample before and after environmental impacts or mechanical stress is already well known in the literature (Saadatfar et al., 2012; Rozenbaum, 2011; Van den Bulcke et al., 2009; Zabler et al., 2008).

The dissolution of carbonates and anhydrite, present as pore-filling cements before the tests, increased rock porosity and surface area. The gain in surface area was caused by an enhanced exposure of small grain-rimming clay minerals to the pore space, which were covered by the pore-filling cements before the experiments and detectable with all methods.

The results from μ-CT analyses and numerical simulations are in accordance with helium porosity and nitrogen permeability measurements. The determination of specific surfaces by BET after Brunauer et al. (1938) and findings by scanning electron microscopy as well as hydro-, mineral- and geochemical analyses of similar sandstones (e.g. Pudlo et al., 2012, 2013, 2015; Henkel, 2016) confirm marked modifications in rock composition induced by CO_2 autoclave experiments. This is most relevant in evaluating the suitability and quality of potential underground reservoirs. Nevertheless the compromise between the representative sample size and the pixel resolution of the μ-CT scans, especially regarding heterogeneities of the sampled material, will still be challenging (Cnudde and Boone, 2013).

In the future, the discussed deviations of data reliability related to grain sizes can be precluded by applying higher scan resolutions and/or smaller sample sizes, following e.g. the approach of Nordahl and Ringrose (2008) to determine an appropriate representative elementary volume (REV) for each sample. This complexity is one of the major topics of the ongoing work by the authors in the HyINTEGER collaborative research project.

Acknowledgements. The authors thank G. Pronk and K. Heister of the Technical University Munich for BET measurements and support. We appreciate funding of the collaborative project H2STORE (grant no. 03SF0434) by the German Federal Ministry of Education and Research (BMBF) within the *Energiespeicher* R&D programme. We also thank the German Federal Ministry for Economic Affairs and Energy for funding the subsequent HyINTEGER project (grant no. 03ET6073). Special thanks go to the industrial partners RWE Gasspeicher GmbH (Dortmund, Germany), GDF Suez E&P Deutschland GmbH (Lingen, Germany), E.ON Gas Storage GmbH (Essen, Germany) and RAG Rohöl-Aufsuchungs Aktiengesellschaft (Vienna, Austria) for sample and data allocation.

Edited by: H. Steeb

References

Brunauer, S., Emmet, P. H., and Teller, E.: Adsorption of gases in multimolecular layers, J. Amer, Chem. Soc., 60, 309–319, 1938.

Cnudde, V. and Boone, M. N.: High-resolution X-ray computed tomography in geosciences: a review of the current technology and applications, Earth Sci. Rev., 123, 1–17, doi:10.1016/j.earscirev.2013.04.003, 2013.

Henkel, S.: Auswirkungen von H_2- und CO_2-Untergrundspeicherungen auf die Reservoireigenschaften von Sandsteinen – Mineralogische Untersuchungen und hochauflösende Computertomographie Modellierungen aus HPHT Autoklaven-Laborexperimenten, Ph.D. thesis, Friedrich Schiller University Jena, Germany, 157 pp., 2016.

Henkel, S., Pudlo, D., Gaupp, R., and H2STORE Team: Research sites of the H2STORE project and the relevance of lithological variations for hydrogen storage at depths, Energy Procedia, 40, 25–33, 2013.

Henkel, S., Pudlo, D., Werner, L., Enzmann, F., Reitenbach, V., Albrecht, D., Würdemann, H., Heister, K., Ganzer, L., and Gaupp, R.: Mineral reactions in the geological underground induced by H_2 and CO_2 injections, Energy Procedia, 63, 8026–8035, 2014.

Henkel, S., Pudlo, D., Albrecht, D., Reitenbach, V., Ganzer, L., and Gaupp, R.: Effects of H_2 and CO_2 underground storage in natural pore reservoirs – Findings by SEM and AFM techniques, in Proceedings of the EAGE – Third Sustainable Earth Science Conference & Exhibition, Celle, Germany, 13–15 October 2015, 5 pp., 2015.

Jovanovic, Z., Khan, F., Enzmann, F., and Kersten, M.: Simultaneous segmentation and beam-hardening correction in computed microtomography of rock cores, Comput. Geosci., 56, 142–150, 2013.

Kieffer, B., Jové, C. F., Oelkers, E. H., and Schott, J.: An experimental study of the reactive surface area of the Fontainebleau sandstone as a function of porosity, permeability, and fluid flow rate, Geochim. Cosmochim. Ac., 63, 3525–3534, 1999.

McBride, E. F.: A classification of common sandstones, J. Sediment. Petrol., 33, 664–669, 1963.

Nordahl, K. and Ringrose, P. S.: Identifying the representative elementary volume for permeability in heterolithic deposits using numerical rock models, Math. Geosci., 40, 753–771, 2008.

Ohser, J. and Mücklich, F.: Statistical Analysis of Microstructures in Material Science, Wiley and Sons, Chichester, 115 pp., 2000.

Panfilov, M.: Underground storage of hydrogen: In situ self-organisation and methane generation, Transport Porous Med., 85, 841–865, 2010.

Parkhurst, D. L. and Appelo, C. A. J.: Description of input and examples for PHREEQC version 3-A computer program for speciation, batch-reaction, one-dimensional transport, and inverse geochemical calculations, US Geological Survey Techniques and Methods, 6, 497 pp., 2013.

Pitzer, K. S., Peiper, J. C., and Busey, R. H.: Thermodynamic properties of aqueous sodium chloride solutions, J. Phys. Chem. Ref. Data, 13, 1–102, 1984.

Pudlo, D., Reitenbach, V., Albrecht, D., Ganzer, L., Gernert, U., Wienand, J., Kohlhepp, B., and Gaupp, R.: The impact of diagenetic fluid–rock reactions on Rotliegend sandstone composition and petrophysical properties (Altmark area, central Germany), Environ. Earth Sci., 67, 369–384, 2012.

Pudlo, D., Ganzer, L., Henkel, S., Kühn, M., Liebscher, A., De Lucia, M., Panfilov, M., Pilz, P., Reitenbach, V., Albrecht, D., Würdemann, H., and Gaupp, R.: The H2STORE Project: Hydrogen underground storage – a feasible way in storing electrical power in geological media? Proceedings of the 3rd Sino-German Conference "Underground Storage of CO_2 and Energy", Goslar, Germany, 21–23 May 2013, 395–412, 2013.

Pudlo, D., Henkel, S., Enzmann, F., Heister, K., Werner, L., Reitenbach, V., Albrecht, D., and Gaupp, R.: The relevance of mineral mobilization and dissolution on the reservoir quality of sandstones in CO_2 storage sites, Energy Procedia, 59, 390–396, 2014.

Pudlo, D., Henkel, S., Reitenbach, V., Albrecht, D., Enzmann, F., Heister, K., Pronk, G., Ganzer, L., and Gaupp, R.: The chemical dissolution and physical migration of minerals induced during CO_2 laboratory experiments: their relevance for reservoir quality, Environ. Earth Sci., 73, 7029–7043, 2015.

Rozenbaum, O.: 3-D characterization of weathered building limestones by high resolution synchrotron X-ray microtomography, Sci. Total Environ., 409, 1959–1966, 2011.

Saadatfar, M., Sheppard, A. P., Senden, T. J., and Kabla, A. J.: Mapping forces in a 3D elastic assembly of grains, J. Mech. Phys. Solids, 60, 55–66, 2012.

Šmigiáň, P., Greksák, M., Kozánková, J., Buzek, F., Onderka, V., and Wolf, I.: Methanogenic bacteria as a key factor involved in changes of town gas stored in an underground reservoir, FEMS Microbiol. Ecol., 73, 221–224, 1990.

Torsaeter, O. and Abtahi, G.: Experimental Reservoir Engineering Laboratory Workbook, Department of Petroleum Engineering and Applied Geophysics, Norwegian University of Science and Technology, 102 pp., 2003.

Van den Bulcke, J., Boone, M. N., Van Acker, J., and Van Hoorebeke, L.: Three-dimensional X-ray imaging and analysis of fungi on and in wood, Microsc. Microanal., 15, 395–402, 2009.

Wentworth, C. K.: A scale of grade and class terms for clastic sediments, J. Geol., 30, 377–392, 1922.

Wiegmann, A.: Computation of the permeability of porous materials from their microstructure by FFF-Stokes, Berichte des Fraunhofer ITWM, Kaiserslautern, Germany, 129, 33 pp., 2007.

Wiegmann, A., Glatt, E., Becker, J., and Westerteiger, R.: PoroDict Tutorial, Calculating pore structure characteristics with PoroDict, Math2Market®, Kaiserslautern, Germany, 53 pp., 2013.

Zabler, S., Rack, A., Manke, I., Thermann, K., Tiedemann, J., Harthill, N., and Riesemeier, H.: High-resolution tomography of cracks, voids and micro-structure in greywacke and limestone, J. Struct. Geol., 30, 876–887, 2008.